Journal of Metals, Materials and Minerals, Vol. 31, No. 4, pp. 95-101, 2021

Controlled plasma tuning of MoS_2 based photodetector: From visible to ultraviolet photo response

Huda Musa MUTLAQ[1,*], and Ali Jabbar FRAIH[1]

[1] *College of Science, Wasit University, Al Kut, Wasit, Iraq*

***Corresponding author e-mail:** hudamusa@uowasit.edu.iq

Received date:
18 July 2021
Revised date
15 September 2021
Accepted date:
17 September 2021

Keywords:
MoS_2;
Oxygen plasma;
Photodetector;
Visible;
Ultraviolet

Abstract

Among diverse family of two-dimensional materials, molybdenum disulfide (MoS_2) is one of the most promising materials for optical applications thanks to its tunable optical energy bandgap. In this work, a MoS_2 based photodetector is fabricated and its optical properties is investigated. With the help of controlled oxygen plasma bombardment, its photoresponse is tuned from visible to ultraviolet region. The photodetector was subjected to three bombardment times of 60 s, 120 s, and 180 s, and it was observed that 180 s irradiation resulted in a change in the optical response range of the photodetector from visible to ultraviolet. In fact, by doping MoS_2 sheets with oxygen ions, they are replaced with sulfur atoms and partially MoS_2 is converted to oxide which its energy band gap increases. Raman analysis shows that the structure of MoS_2 is preserved even after plasma irradiation. However, due to the bombardment, response time of the tuned photodetector is slowed down due to the increase of trap states.

1. Introduction

The emergence of unique properties in two-dimensional (2D) materials has made them very promising for electronic and optoelectronic applications [1]. In this regards, transition metal dichalcogenides (TMDs) as optically active 2D materials, have attracted considerable attention [2]. TMDs are a group of 2D materials with MX_2, which M is a transition metal atom and X is a chalcogen atom [3]. In this structure, the transition metal atom is sandwiched between two chalcogen atoms. These materials have an indirect energy gap in bulk crystal, but are interestingly converted to a direct energy gap in monolayer [4]. Today, many layered TMDs have been introduced, such as: molybdenum disulfide (MoS_2) [5,6], Tungsten disulfide (WS_2) [7], Molybdenum ditelluride ($MoTe_2$) [8] and so forth [2]. Among the attractive structures of TMDs, more attention is allocated to MoS_2 where it is dramatically used in optoelectronic applications [9].

Mono- and few- layers of MoS_2 are synthesized in different ways, the most important of which are: mechanical exfoliation [10], sonication-assisted solvent exfoliation [11], and solid gas reaction of Mo powders [12,13]. The solvent-based sonication method has received more attention due to its easy, cheap and mass production of mono- and few- layers of MoS_2 [11].

Molybdenum has historically been used as lubricant and catalysis, but today it is increasingly employed in optoelectronic devices such as photodetectors [14], solar cells [15], and light emitting diodes [16] due to its high carrier mobility, modulated energy band gap, and light-matter interaction[11,14,15,17]. MoS_2 based photodetectors show the ability to detect light in the visible range with a photoresponsivity of up to 1000 A/W and a response time of few microseconds [18,19].

MoS_2-based photodetectors cover a wide photodetection range from visible to ultraviolet regions and are not suitable for detecting specific wavelengths [19]. Moreover, few number of research have been reported so far on 2D material based photodetectors for the ultraviolet region. Therefore, with energy bandgap engineering, it could be possible to develop a MoS_2 based photodetector that could operate only in the ultraviolet area. One of the methods that can be used to change the band gap of MoS_2 is oxygen plasma bombardment. In general, oxygen plasma can both etch and oxidize the layer. Ghasemi *et al*. have shown that oxygen plasma can etch MoS_2 layers with a slow rate [20]. Thus, the applying oxygen plasma can etch some MoS_2 layers, but its major contribution will be in oxidizing the layers and increasing the energy band gap.

In this work, MoS_2 nanosheets were synthesized by sonication in NMP solvent and then deposited on pre-patterned gold electrodes. SEM, TEM, AFM, Raman and UV-Visible absorption analyzes were used to investigate the layered structure of nanosheets. After evaluating the optoelectronic properties of the MoS_2 photodetector, it was exposed to 200 W of oxygen plasma and showed that as the bombardment time increased to 180 s, the photoresponse of the MoS_2 is shifted from visible to ultraviolet region. In fact, oxygen bombardment replaces oxygen with sulfur atoms, and the band gap increases in MoS_2 and as a result it shows photoresponse only to higher-energy photons.

2. Experimental

2.1 Material supplies

MoS_2 powder with purity more than 99% and N-Methyl-2-pyrrolidone (NMP) solvent were purchased from Sigma-Aldrich.

2.2 Material characterizations

TEM image was recorded by CM30, Philips microscope at operating voltage of 150 kV. Hitachi-S4160 SEM microscope was used to take the image of the device and sheets. Height profile of MoS_2 sheets were measured by NT-MDT AFM microscope in non-contact mode. Raman spectra of the samples were taken by Senterra Raman microscope spectrometer (532 nm laser). X-ray diffraction (XRD) analysis were performed using a Panalytical X'Pert PRO MPD system. A PG Instrument Ltd spectrophotometer was utilized to collect UV−visible absorption spectra. Electrical measurements were done with Keithly 2450 source measure unit in dark and under various laser illuminations at room ambient.

2.3 Synthesis of MoS_2 few layers

1 g of MoS_2 powders and 100 mL of NMP were mixed and stirred for 10 min. The solution was then exposed to a 300 W probe sonication for one hour. An ice bath was used to prevent the solution from heating up. The resulting solution was then centrifuged at 2000 rpm for 30 min, and top two-thirds of the obtained solution was collected for device fabrication and analysis.

3. Results and discussion

The solution containing MoS_2 nanosheets was prepared by sonication method in NMP solvent [21]. SEM, TEM and Raman analyzes were used to characterize it. Figure 1(a) presents the SEM image of MoS_2 sheets on a substrate. The sheets cover the entire surface and their approximate dimensions are about a few micrometers. Figure 1(b) shows the TEM image of a multilayer MoS_2 sheet on a grid. The edge of the sheet well prove its layered structure [11]. Figure 1(c) demonstrates the 3D image measured by the AFM analysis for deposited sheets on a substrate. According to it, thickness of the sheets is less than 30 nm.

Figure 2(a) shows the Raman spectrum of the MoS_2 sheets on the substrate. The Raman spectrum of the multilayer MoS_2 consists of two peaks: the E^1_{2g} peak at position ~385 cm^{-1}, which is due to phonon oscillations inside the plane, and the A_{1g} peak at position ~407 cm^{-1}, which is due to phonon oscillations outside the plane [20]. Schematics of oscillation modes are also drawn in the Figure 2(a). Figure 2(b) shows the absorption spectrum of the NMP solution containing MoS_2 sheets. Accordingly, MoS_2 has a relatively good absorption in the range of 200 nm to 800 nm. Multilayers of MoS_2 also show two absorption peaks at 610 nm and 670 nm, called B and A peaks, respectively [22]. These two peaks are due to the direct transition of carriers at K point in the Brillouin zone [13]. There is also a strong absorption in the range of 390 nm to 500 nm in the spectrum due to the direct transitions of the carriers from the deep valence bands to the conduction band [23,24].

Figure 3 shows the fabrication process of the MoS_2 based photodetector. Accordingly, 300 nm of oxide was first grown on the silicon substrate. Then 100 nm of gold was deposited on the oxide layer (Figure 3(a)). By using a photolithography process, the gold layer was patterned and washed with acetone (Figure 3(b)). Next, a few drops of the MoS_2 solution were deposited on the sample (Figure 3(c)) and allowed to be dried at room temperature (Figure 3(d)).

Figure 4(a) displays the SEM image of the fabricated photodetector. Multi-layer of MoS_2 are deposited on the channel of the photodetector which connect the source and drain electrodes. The width of the channel is about 5 μm. Figure 4(b) shows the electrical properties of the photodetector. In dark, a current of about 3 μA passes through channel of the photodetector in the applied voltage range of -3 V to +3 V. Moreover, under 405 nm, 532 nm and 655 nm laser illuminations (with power of 1 mW) the current passing through the device channel increases. The highest photocurrent was observed for 405 nm and the lowest photocurrent for 655 nm. For 405 nm, photons generate more photocurrent due to their higher energy while in the case of 655 nm, photons generate less photocurrent as a result of their lower energy. However, the MoS_2-based photodetector shows that it responds well to 405 nm, 532 nm and 655 nm lasers, generating photocurrent in all three cases.

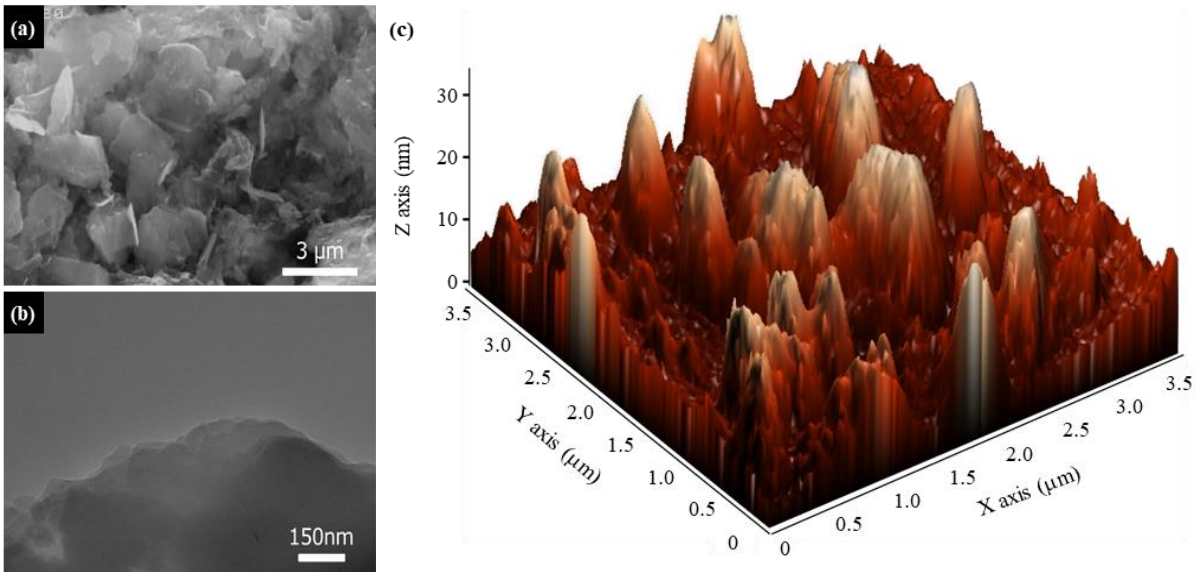

Figure 1. (a) SEM image of the deposited MoS_2 sheets, (b) TEM image of a multilayered MoS_2 sheet, and (c) AFM 3d-image of the deposited MoS_2 sheets on a substrate.

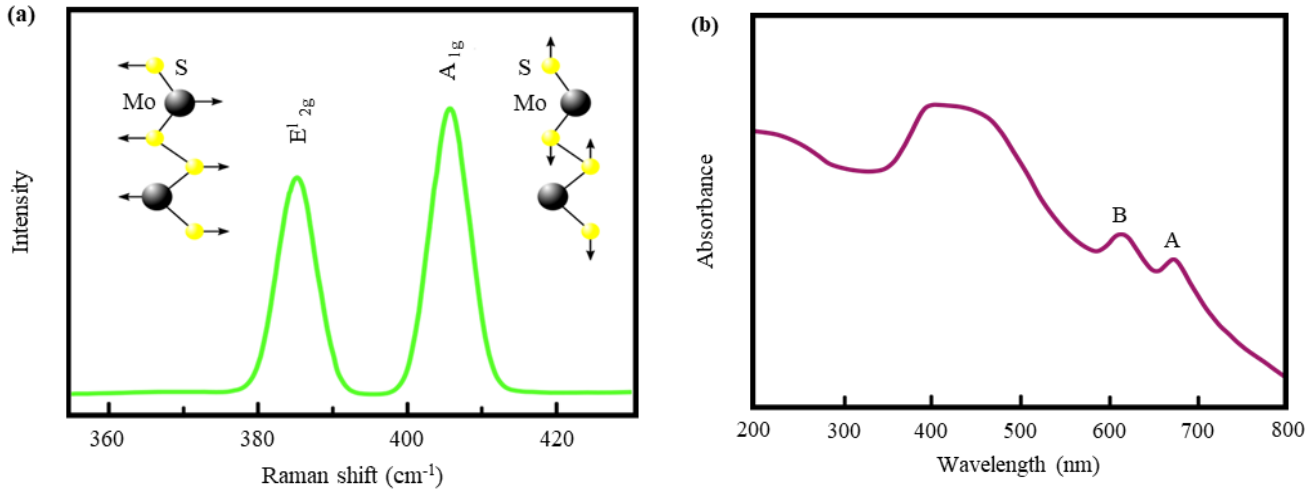

Figure 2. (a) Raman spectrum of the MoS_2 multilayers and their corresponding oscillation modes, and (b) UV-Visible absorption spectrum of the MoS_2 solution.

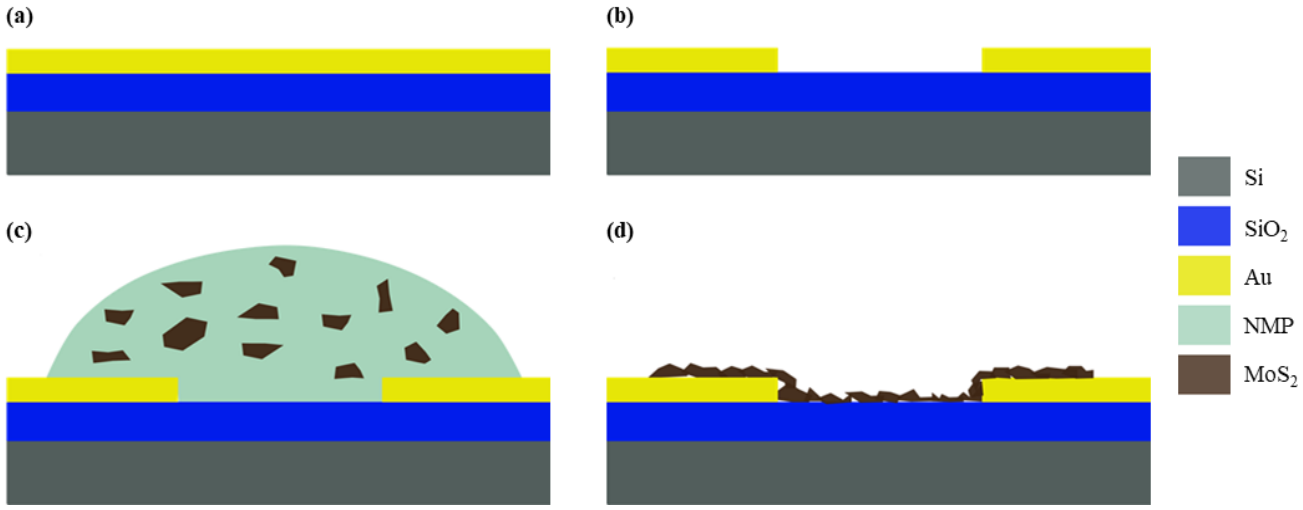

Figure 3. Fabrication process of the MoS_2 based photodetector: (a) Depositing of 100 nm gold on an oxide substrate, (b) Patterning of gold film by photolithography method, (c) Casting of MoS_2 solution on electrode, and (d) Drying the solution and drying the device.

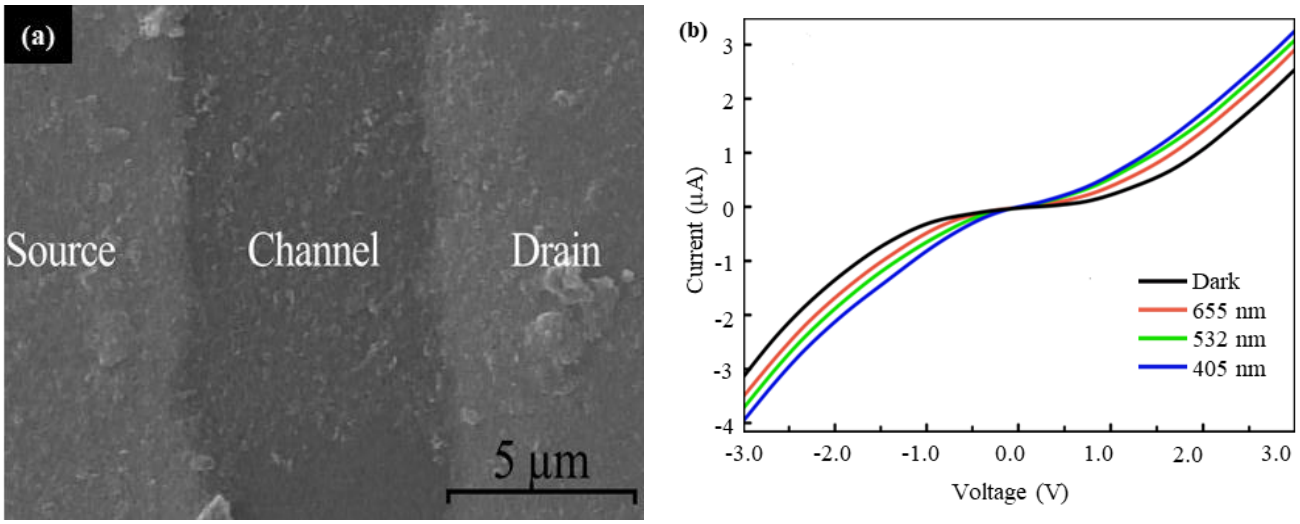

Figure 4. (a) SEM image of the fabricated MoS_2 based photodetector, and (b) I-V curves of the device in dark and under 405 nm, 532 nm, and 655 nm laser illumination with power of 1 mW.

In the next step, the effect of oxygen plasma bombardment on the optoelectronic performance of the MoS_2 based photodetector was investigated. Figure 5(a) shows a schematic of the bombardment process. In order to prevent the negative effect of plasma on electrical contacts, the surface of the source and drain electrodes was passivated with epoxy glue. The device was then placed inside a quartz tube and oxygen gas with a flow of 20 sccm was introduced to bring the chamber pressure to 90 torr. Then 200 W oxygen plasma was applied to the samples in three times of 60 s, 120 s and 180 s and their electrical and optical properties were investigated. Figure 5(b) presents the current-voltage curves of the devices after each stage of oxygen bombardment. It is observed that with increasing plasma time, the electrical resistance of the channel increases and less current passes through the channel. It is possible that the underlying MoS_2 layers of the channel, which remain intrinsic, are responsible for the passage of current. However, these underlying layers are less involved in the photocurrent generation process, and most of the photoexcited carriers generate in the upper layers. Then, the performance of the devices was examined under the irradiation of 405 nm, 532 nm and 655 nm lasers at 5 V biasing voltage and 5 mW output power. Figure 5(c) demonstrates the current-time characteristics of all four photodetectors of MoS_2, 60-MoS_2, 120-MoS_2 and 180-MoS_2. For 405 nm radiation, photocurrent is generated in all four devices. The highest value is for as-prepared MoS_2 photodetector and the lowest is for 180-MoS_2. However, they all respond to 405 nm light. At 532 nm laser radiation, photocurrents are generated in MoS_2, 60-MoS_2, and 120-MoS_2 devices, but it is observed that the 180-MoS_2 sample does not show any optical response. A similar trend is observed for 655 laser radiation and no response is observed for the 180-MoS_2. Therefore, the 180-MoS_2 sample shows only an optical response under 405 nm illumination and no response is observed for longer wavelengths. Oxidation of the upper sheets of the channel and their local conversion to oxide is the reason for this behavior of 180-MoS_2 photodetector. Since the upper layers have the highest optical absorption, their oxidation will increase the chances of absorbing higher energy photons, while light illumination with higher wavelengths will have less absorption. As a result, the selectivity of the 180-MoS_2 photodetector will increase to 405 nm laser, and therefore will not respond to higher wavelengths. It should be noted that increasing the bombardment time beyond 180 s will etch the sheets and break down the electrical connection of the channel and the photodetector can no longer be used.

Figure 6(a) schematically shows the effect of oxygen bombardment on MoS_2 sheets. We believe that oxygen plasma leads to the oxidation of the upper layers of MoS_2, which play a major role in the absorption of light and the optical response of photodetectors. Figure 6(b) shows the SEM image of channel after 180 s of plasma bombardment. Accordingly, no significant etching effect is observed in the channel and most of the channel is covered by MoS_2 layers, even after plasma treatment. Figure 6(c) and (d) show XPS spectra of 2p orbital of sulfur in both MoS_2 and 180-MoS_2 samples with two peaks at around 164.3 eV and 163.1 eV corresponding $2P_{1/2}$ and $2P_{3/2}$ states. In the 180-MoS_2 sample, in addition to these two peaks, another peak is observed around 165.4 eV, which is due to O-S bonds and indicates that the surface of the MoS_2 layers has been oxidized and the O-S bonds have increased.

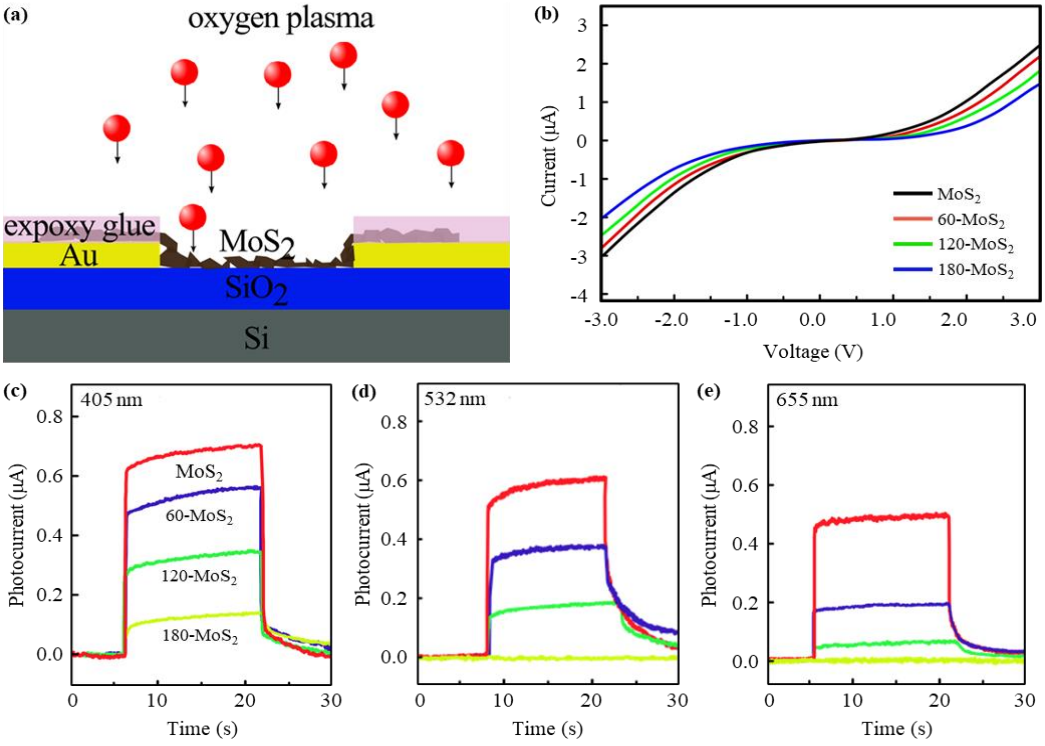

Figure 5. (a) Schematic of oxygen plasma bombardment of the MoS_2 based photodetector, (b) I-V curves of the MoS_2 and treated photodetectors, (c) Time trace measurement of the MoS_2 and treated photodetectors under 405 nm laser illumination (5 mW) at biasing voltage of 5 V, (d) Time trace measurement of the MoS_2 and treated photodetectors under 532 nm laser illumination (5 mW) at biasing voltage of 5 V, and (e) Time trace measurement of the MoS_2 and treated photodetectors under 655 nm laser illumination (5 mW) at biasing voltage of 5 V.

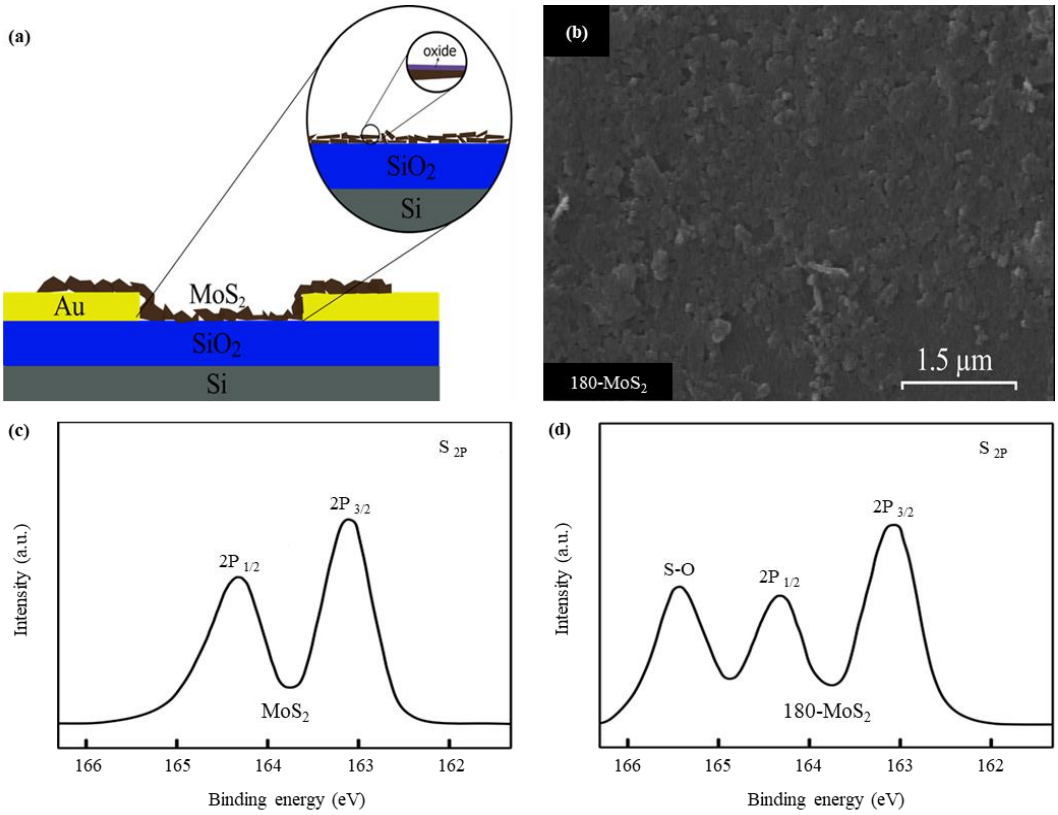

Figure 6. (a) Schematic of plasma treatment of MoS_2 sample and corresponding local oxidation, (b) SEM image of channel of 180-MoS_2 photodetector, (c) XPS spectrum of 2p orbital of sulfur in MoS_2 sample, and (d) XPS spectrum of 2p orbital of sulfur in 180-MoS_2 sample.

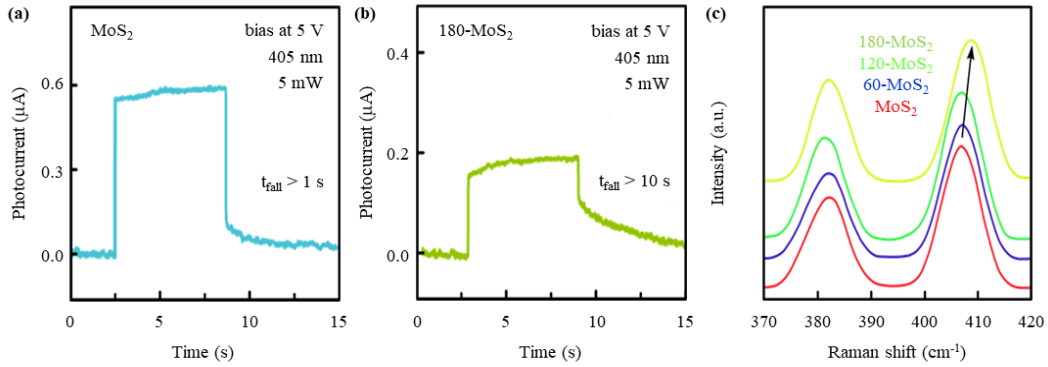

Figure 7. (a) Time trace measurement of the MoS_2 based photodetector under 405 nm illumination and operating voltage of 5 V, (b) Time trace measurement of the 180 s bombarded MoS_2 based photodetector under 405 nm illumination and operating voltage of 5 V, and (c) Raman spectra of the pristine MoS_2, 60 s, 120 s, and 180 s bombarded MoS_2 samples.

Figure 7(a) shows the time trace response the MoS_2 based photodetector under 405 nm light illumination. The fall time of the photodetector was measured about 1.4 s, which refers to time taken for the current to return to its baseline. In the case of 180-MoS_2, shown in Figure 7(b), this time increases to more than 10 s due to the occurrence of trap states caused by oxygen bombardment [23,25]. Figure 7(c) compares the Raman spectrum of intrinsic MoS_2 and bombarded MoS_2 samples. According to the figure, as the bombing time increases, the general characteristics of the two E^1_{2g} and A_{1g} peaks are preserved, but the A_{1g} peak gradually shifts from 407 cm^{-1} to 409 cm^{-1} due to the removal of sulfur atoms in the upper MoS_2 layers in the channel of the photodetectors [20].

The results of various analyses lead to the following conclusion. Applying of oxygen plasma leads to oxidation of the upper layers of MoS_2 in the channel. SEM images before and after plasma treatment indicate that etching has not occurred, which is consistent with the work of others [20]. Raman analysis also shows that the whole plasma treated layer still has the property of MoS_2 and XPS analysis proved that the upper layer of MoS_2 are oxidized. Therefore, the results are completely consistent with our claim that only the upper layers, which play a significant role in the optical absorption of the photodetector, are oxidized and lead to a change in the energy band gap of the MoS_2.

4. Conclusions

MoS_2 is widely used in optoelectronic devices due to its attractive optical properties. In this work, multilayers of MoS_2 sheets were prepared by sonication method and then a MoS_2-based photodetector was fabricated. SEM, TEM, AFM, Raman, XPS, and UV-Visible analyzes were used to control the photodetector fabrication process. The electrical and optical properties of the photodetector were then evaluated under 405 nm, 532 nm and 655 nm laser illuminations. Then, the photodetector was exposed to 200 W oxygen plasma for 60 s, 120 s and 180 s and the optical response of the photodetectors was studied at each stage. It was observed that in 180 s of radiation, the photodetector responds only to the 405 nm laser irradiation and no response is detected for longer wavelengths. Although, Raman analysis shows that the MoS_2 characteristic is preserved even after bombardment, the photo response region of the photodetector was tuned from visible to ultraviolet regions thanks to local oxidation of the MoS_2 sheets.

References

[1] T. Tan, X. Jiang, C. Wang, B. Yao, and H. Zhang, "2D material optoelectronics for information functional device applications: status and challenges," *Advanced Science*, vol. 7, no. 11, pp. 2000058, 2020.

[2] Q. Fu, J. Han, X. Wang, P. Xu, T. Yao, J. Zhong, W. Zhong, S. Liu, T. Gao, Z. Zhang, L. Xu, and B. Song, "2D transition metal dichalcogenides: Design, modulation, and challenges in electrocatalysis," *Advanced Materials*, vol. 33, no. 6, pp. 1907818, 2020.

[3] R. Ge, X. Wu, L. Liang, S. M. Hus, Y. Gu, E. Okogbue, H. Chou, J. Shi, Y. Zhang, S. K. Banerjee, Y. Jung, J. C. Lee, and D. Akinwande, "A library of atomically thin 2D materials featuring the conductive-point resistive switching phenomenon," *Advanced Materials*, vol. 33, no. 7, pp. 2007792, 2020.

[4] A. Maniyar, and S. Choudhary, "Visible region absorption in TMDs/phosphorene heterostructures for use in solar energy conversion applications," *RSC Advances*, vol. 10, no. 53, pp. 31730-31739, 2020.

[5] J. Jiang, Z. Chen, Y. Hu, Y. Xiang, L. Znang, Y. Wang, F-C. Wang, and J. Shi, "Flexo-photovoltaic effect in MoS_2," *Nature Nanotechnology*, vol. 16, pp. 894-901, 2021.

[6] F. Ghasemi, and M. Hassanpour Amiri, "Facile in situ fabrication of rGO/MoS_2 heterostructure decorated with gold nanoparticles with enhanced photoelectrochemical performance," *Applied Surface Science*, vol. 570, pp. 151228, 2021.

[7] H. Xia, Z. Chen, S. Luo, F. Qin, A. Idelevich, S. Ghosh, T. Ideue, Y. Iwasa, A. Zak, R. Tenne, Z. Chen, W-T. Liu, and S. Wu, "Probing the chiral domains and excitonic states in individual WS2 tubes by second-harmonic generation," *Nano Letters*, vol. 21, no. 12, pp. 4937-4943, 2021.

[8] C. Li, R. Tian, R. Yi, S. Hu, Y. Chen, Q. Yuan, X. Zhang, Y. Liu, Y. Hao, X. Gan, and J. Zhao, "$MoTe_2$ PN homojunction constructed on a silicon photonic crystal cavity for high-performance photodetector," *ACS Photonics*, 2021.

[9] Y. Yang, Z. Liu, K. Shu, L. Li, and J. Li, "Improved performances of CVD-grown MoS_2 based phototransistors enabled by encapsulation," *Advanced Materials Interfaces*, vol. 8, no. 11, pp. 2100164, 2021.

[10] M. Krawczyk, M. Pisarek, R. Szoszkiewicz, and A. Jablonski, "Surface characterization of MoS_2 atomic layers mechanically exfoliated on a Si substrate," *Materials*, vol. 13, no. 16, pp. 3595, 2020.

[11] F. Ghasemi, and S. Mohajerzadeh, "A sequential solvent exchange method for controlled exfoliation of MoS_2 suitable for phototransistor fabrication," *ACS Applied Materials & Interfaces*, vol. 8, no. 45, pp. 31179-31191, 2016.

[12] M. Demirtaş, C. Odacı, Y. Shehu, N. K. Perkgöz, and F. Ay, "Layer and size distribution control of CVD-grown 2D MoS_2 using ALD-deposited MoO_3 structures as the precursor," *Materials Science in Semiconductor Processing*, vol. 108, pp. 104880, 2020.

[13] F. Ghasemi, R. Frisenda, D. Dumcenco, A. Kis, D. Perez de Lara, and A. Castellanos-Gomez, "High throughput characterization of epitaxially grown single-layer MoS_2," *Electronics*, vol. 6, no. 2, pp. 28, 2017.

[14] W. Wang, X. Zeng, J. H. Warner, Z. Guo, Y. Hu, Y. Zeng, J. Lu, W. Jin, S. Wang, J. Lu, Y. Zeng, and Y. Xiao, "Photo-response-Bias modulation of a high-performance MoS_2 photo-detector with a unique vertically stacked 2H-MoS_2/1T@ 2H-MoS_2 structure," *ACS Applied Materials & Interfaces*, vol. 12, no. 29, pp. 33325-33335, 2020.

[15] D. H. Shin, J. S. Ko, S. K. Kang, and S.-H. Choi, "Enhanced flexibility and stability in perovskite photodiode–solar cell nanosystem using MoS2 electron-transport layer," *ACS applied materials & interfaces*, vol. 12, no. 4, pp. 4586-4593, 2020.

[16] R. Sorrentino, R. Worsely, P. Lagonegro, C. Martella, A, Alieva, G. Scavia, F. Galeotti, M. Pasini, B. Dubertret, S. Brovelli, A. Molle, C. Casiraghi, and U. Giovanella, "Hybrid MoS_2/PEDOT: PSS transporting layer for Interface engineering of nano-platelets based light-emitting diodes," *Dalton Transactions*, vol. 26, 2021.

[17] F. Ghasemi, A. Abdollahi, A. Abnavi, S. Mohajerzadeh, and Y. Abdi, "Ultrahigh sensitive MoS_2/rGo Photodetector based on aligned CNT contacts," *IEEE Electron Device Letters*, vol. 39, no. 9, pp. 1465-1468, 2018.

[18] W. Chen, W-Y. Yin, W-S. Zhao, R. Hao, E. Li, K. Kang, and J. Guo, "Scaling analysis of high gain monolayer MoS_2 photo-detector for its performance optimization," *IEEE Transactions on Electron Devices*, vol. 63, no. 4, pp. 1608-1614, 2016.

[19] P. Gant, P. Huang, D. P. de Lara, D. Guo, R. Frisenda, and A. Castellanos-Gomez, "A strain tunable single-layer MoS_2 photo-detector," *Materials Today*, vol. 27, pp. 8-13, 2019.

[20] F. Ghasemi, A. Abdollahi, and S. Mohajerzadeh, "Controlled plasma thinning of bulk MoS_2 flakes for photodetector fabrication," *ACS Omega*, vol. 4, no. 22, pp. 19693-19704, 2019.

[21] F. Ghasemi, M. Jalali, A. Abdollahi, S. Mohammadi, Z. Sanaee, and S. Mohajerzadeh, "A high performance supercapacitor based on decoration of MoS_2/reduced graphene oxide with NiO nanoparticles," *RSC Advances*, vol. 7, no. 83, pp. 52772-52781, 2017.

[22] C. Trovatello, H. P. C. Miranda, A. Malina-Sanchez, R. Borrego-Varillas, C. Manzoni, L. Moretti, L. Ganzer, M. Maiuri, J. Wang, D. Dumcenco, A. Kis, L. Wirtz, A. Marini, G. Soavi, A. C. Ferrari, G. Cerullo, D. Sangalli, and S. D. Conte, "Strongly coupled coherent phonons in single-layer MoS_2," *ACS nano*, vol. 14, no. 5, pp. 5700-5710, 2020.

[23] F. Ghasemi, "Vertically aligned carbon nanotubes, MoS_2–rGo based optoelectronic hybrids for NO_2 gas sensing," *Scientific Reports*, vol. 10, no. 11306, 2020.

[24] L. T. Manamel, S. C. Madam, S. Sagar, and B. C. Das, "Electro-forming-free nonvolatile resistive switching of redox-exfoliated MoS_2 nanoflakes loaded polystyrene thin-film with synaptic functionality," *Nanotechnology*, vol. 32, no. 35, pp. LT02, 2021.

[25] X. Liu, S. Hu, J. Luo, X. Li, J. Wu, D. Chi, K-W. Ang, W. Yu, and Y. Cai, "Suspended MoS_2 photodetector using patterned sapphire substrate," *Small*, no. 2100246, 2021.